Determining the Low-Temperature Fracture Toughness of Asphalt Mixtures

Revision submission date: November 15th, 2001

Word count: 4640 plus 2 tables and 8 figures

Submitted to

The Transportation Research Board

for Presentation and Publication

by

Dr. Mihai O. Marasteanu
Assistant Professor, University of Minnesota
500 Pillsbury Drive S.E., Minneapolis, MN 55455
Telephone: (612) 625-5558, E-mail: maras002@tc.umn.edu

Dr. Joseph F. Labuz
Associate Professor, University of Minnesota
500 Pillsbury Drive S.E., Minneapolis, MN 55455
Telephone: (612) 625-9060, E-mail: jlabuz@tc.umn.edu

Dr. Shongtao Dai
Research Operations Engineer, Office of Materials and Road Research
Minnesota Department of Transportation, Maplewood, MN 55109
Tel: 651-779-5218, E-mail: shongtao.dai@dot.state.mn.us

Xue Li
Graduate student, University of Minnesota
500 Pillsbury Drive S.E., Minneapolis, MN 55455
Telephone: (612) 625-1571, E-mail: lixx0384@umn.edu

ABSTRACT
There has been a sustained effort in applying fracture mechanics concepts to crack formation and propagation in bituminous pavement materials. Adequate fracture resistance is an essential requirement for asphalt pavements built in the northern part of the US and Canada for which the prevailing failure mode is cracking due to low-temperature shrinkage stresses. The current Superpave specifications address this issue mainly through the use of strength tests on un-notched (smooth boundary) specimens. However, recent studies have shown the limitations of this approach and have suggested that fracture mechanics concepts, based on tests performed on notched samples, should be employed instead.

Research in progress at University of Minnesota investigates the use of fracture mechanics principles to determine the low-temperature fracture properties of asphalt mixtures. This paper presents a testing protocol that allows obtaining multiple measurements of fracture toughness as a function of crack propagation based on the compliance method to measure crack length. An increase in fracture toughness with crack length is observed, which is consistent with the behavior displayed by other brittle materials. The plateau of the curves may be representative of the asphalt concrete resistance to fracture because the initial values can be significantly influenced by the presence of the inelastic zone at the crack tip.

INTRODUCTION

Adequate fracture resistance is essential for asphalt pavements built in the northern part of the U.S. and in Canada for which the prevailing failure mode is cracking due to low-temperature shrinkage stresses. The current Superpave specifications address this issue through the use of strength and creep tests performed on smooth boundary specimens, that is, specimens without a notch.

An increasing number of researchers realized the limitations associated with predicting fracture properties based on tests performed on un-notched samples. As a consequence, a number of studies started to investigate the application of fracture mechanics concepts to the behavior of bituminous materials. One of the first attempts to test notched beams of asphalt mixtures at low temperatures predates SHRP (1). However, the use of a fracture mechanics approach in bituminous material research did not become significant until after the end of SHRP.

Early work on the application of fracture mechanics concepts to the behavior of bituminous materials comes from the Chemistry Department of Queens University in Canada. Hesp and his collaborators were some of the first investigators to publish on the use of a simple test to measure the plane strain fracture toughness of asphalt binders in three-point bending (2, 3). The proposed test follows closely with the ASTM E399 standard for testing metals that assumes the material to be linear elastic (4). Other researchers used the method developed by Hesp in their fracture studies (5, 6).

One of the drawbacks of fracture toughness measurements based on the ASTM E399 test method is the limitation of linear elastic behavior. Another is the difficulty in accurately measuring the crack length used in the K_{IC} calculation. Recent work by Hesp and Roy (7) address these issues through the use of elasto-plastic fracture mechanics concepts. In their approach, they proposed the use of the crack tip opening displacement (CTOD) method to describe the fracture properties of materials that exhibit time-independent, non-linear behavior. Due to the less restrictive requirements and the ability to predict failure conditions even when

crack tip plasticity occurs, the CTOD concept has been used for both metal and plastic materials (8, 9).

In a number of recent papers, Roque and collaborators have investigated the use of the indirect tension test (IDT) to determine fracture properties of asphalt mixtures (10, 11). In their research they used the regular IDT cylindrical specimens with an 8-mm diameter hole drilled in the center. Their research focused on obtaining suitable crack growth rate parameters to describe the fatigue cracking of asphalt mixtures under traffic loading at intermediate temperatures.

SCOPE

Research in progress at University of Minnesota investigates the use of laboratory testing to determine the low-temperature fracture properties of asphalt mixtures. The approach used in a previous research effort by Labuz and Dai (12), which is to measure the crack resistance curve, is one of the methods under investigation. The focus of this paper is to describe the procedure used in this previous research effort and to present some of the relevant results from the R-curve analysis.

FRACTURE MECHANICS

Because fracture mechanics specifically describes the energy required for cracks to initiate, fracture tests differ from conventional strength tests by requiring that the specimen have a well-defined crack. The elastic stress field can be calculated in a two dimensional body of arbitrary size and shape in any mode of loading. For the Cartesian coordinate system at the crack tip, the near tip stress field can be expressed as

$$\sigma_{ij} = \frac{K_I}{(2\pi r)^{1/2}} f_{ij}(\theta) \qquad (1)$$

where σ_{ij} are the stresses acting on a material element at a small distance r from the crack tip at an angle θ from the crack plane, and $f_{ij}(\theta)$ are known functions of θ. The stress intensity factor, K_I is dependent on the specimen geometry and loading. The term $K_I/\sqrt{2\pi r}$ must have the dimensions of stress, or K_I must have the dimensions of stress times the square root of length.

The fracture will extend when K_I reaches a critical value called the fracture toughness K_{Ic}. Fracture mechanics may provide a method to establish, in quantitative terms, the effects that composition, stress path or heat treatment have on the service and performance of asphalt concrete. Fracture testing can be used to determine the suitability of a material for a specific application where the stress conditions are prescribed and where a maximum flaw size (crack length) can be established.

For linear fracture mechanics to apply, the size of the nonlinear region at the crack tip induced by the singular stress field must be negligible in comparison with the crack length and other dimensions of the body. Investigators (13, 14) have shown that linear elasticity is an acceptable assumption for rock-like materials if the scale or specimen size is sufficiently large. Of course, the scale is dependent on the material.

Consider a structure containing a crack that is subjected to mode I loading under controlled displacement conditions; some nonlinear behavior prior to the limit load (point A in Figure 1a) may be present due to the severe stress concentration at the crack tip. If the specimen is unloaded and no crack growth occurs during unloading, then the unloading path should be a

straight line. In addition, if the crack closes completely such that no permanent or plastic deformation occurs, then the path should return to the origin.

If the specimen is displaced to a point further past A, say to C in Figure 1a, and produces a crack extension, then energy ΔU is consumed in advancing the crack a distance Δa, where the shaded area OAC is given by

$$\Delta U = \frac{1}{2} F_{avg} \Delta u \qquad (2)$$

where F_{avg} is the average load between points A and C and Δu is the load-point displacement between points A and C at the average load. The elastic energy contained in the specimen is represented by the area OAB, but once the crack extends over a length Δa the stiffness of the specimen will decrease to that represented by line OC. Thus, crack propagation from a to a + Δa will result in elastic energy release from the specimen equal in magnitude to the area OAC, which may be thought of as the fracture energy. The energy can also include some irrecoverable work (see Figure 1b). This may be interpreted as the fracture energy using a nonlinear fracture mechanics approach.

In experiments for determining fracture toughness, the applied load is directly measured. However, the crack extension Δa is generally microscopic in size, concealed by the sample, or is just difficult to estimate. An indirect measure of crack length was developed by Irwin and Kies (15) and is known as the compliance method. To apply the compliance method to a given testing geometry and loading configuration, it is important to show that the specimen behaves according to linear elastic fracture mechanics and that the compliance is independent of material properties. Once this has been established the stress intensity factor K_I can be calculated.

The energy release per unit crack extension G_I is given by

$$G_I = \frac{\Delta U}{B \cdot \Delta a} \qquad (3)$$

where B is the specimen thickness. The incremental change in the load- displacement response of the test specimen is known as the compliance λ for a given specimen geometry and loading configuration:

$$\lambda_i = \frac{\Delta u}{F_{avg}} \qquad (4)$$

where λ_i is the initial compliance. The tangent of the initial load-displacement slope will provide a value for the initial compliance. A method for obtaining the initial compliance of a specimen is to load the specimen incrementally and plot the load versus load-point displacement. For non-ideal brittle materials such as asphalt concrete, nonlinear processes occur such that some residual displacement of the load point is observed following a load-unload cycle (see Figure 1b). So as seen by comparing Figure 1a for an ideal material with Figure 1b for non-ideal materials, some corrections may be warranted to adjust for these nonlinearities and hysteresis effects in evaluating fracture toughness of non-ideal materials. Combining equations (3) and (4):

$$\Delta U = \frac{1}{2} F_{avg}^2 \cdot \lambda_i \qquad (5)$$

Substituting ΔU from equation (3) and taking the limit as the incremental change in crack length Δa approaches zero yields

$$G_I = \frac{1}{2B} F^2 \frac{d\lambda}{da} \quad (6)$$

where F is the load evaluated at the critical crack length a. It can be shown that the energy release rate G_I is related to the stress intensity factor K_I by

$$K_I = \left[\frac{G_I E}{(1-\upsilon^2)}\right]^{1/2} \quad (7)$$

where E is Young's modulus and ν is Poisson's ratio

EXPERIMENTAL PROCEDURE

Load Apparatus and Instrumentation

A closed-loop servo-hydraulic 1 MN (220 kips) load frame (MTS Systems) was used to perform the tests, with the crack mouth opening displacement (CMOD) as the feedback signal. The CMOD was measured by a clip gage and the CMOD was programmed to increase at a constant rate of 10^{-4} mm/s. An unload-reload procedure was used at the start of the test to determine an accurate value of initial compliance. Three-point-bend testing requires that a compressive load be applied to the beam surface opposite the notch. The loading fixture is designed to minimize frictional effects through the use of rollers (as suggested by ASTM E399). The entire support fixture was constructed of stainless steel. The initial roller position is maintained by soft springs and backstops, which establish the test span dimension. The support rollers are allowed to rotate out away from the backstops during the test but will remain in contact with the sample. The roller support blocks are secured to a 12.7 mm thick base plate with a 9.5 mm diameter dowel hole for alignment with the actuator center. The span dimension is set at 4.0 times the beam height.

To obtain an accurate measure of the load-point displacement (LPD), a reference frame called the saddle (shown in Figure 2 for a core specimen), supported by the sample at the locations opposite the support rollers, was designed. The saddle allows the upper loading roller to pass freely through the plate and provides a location for two linear variable differential transformers (LVDTs) to measure the load-point displacement. The saddle for this work was constructed of a 12.7 mm thick, 209.6 x 133.4 mm stainless steel plate. The roller opening was cut to 1.3 mm larger than the loading roller to allow friction-free movement. The saddle will remain parallel to the original core axis during the loading process (unless crushing of the specimen on the support rollers occurs) with the saddle supported on the specimen by leveling screws directly over the support rollers.

To successfully measure the load-point displacement with the saddle as the reference frame, contact with some portion of the specimen is required. In this design the LVDT platen and yoke (shown in Figure 3 for a core specimen), makes contact with the notch front. The yoke is made of a thin but stiff piece of stainless steel. Two LVDT platens are secured to the shoulders of the yoke. The two LVDTs measure the displacement of the notch front at two points relative to the saddle. The signal from the two LVDTs is acquired separately but averaged to correct for twisting of the specimen. Special brass LVDT holders shown in Figure were made for the RDP 1000 series LVDTs. The 1.6 mm (1/16 in.) thick brass sleeve is split for flexibility

and has a 3.2 mm (1/8 in.) wide collar to butt against the saddle. A setscrew is placed within the side of the saddle adjacent to the LVDT to clamp the brass sleeve and LVDT into position.

All transducers (load cell, clip gage and two LVDTs) were calibrated prior to testing. The load cell was a Lebow 22.5 kN cell model-3132; the clip gage, an MTS clip-on gage model 632-02B-20; and the two LVDTs, RDP model-GTX1000. The load cell has a linear range of 22.5 kN (5 kips) and was periodically calibrated using a proving ring at room temperature. The clip gage has a linear range of 2.5 mm (0.1 in.) and was calibrated using a Schaevitz 41M calibration micrometer and a clip gage stand. The clip gage and MTS 448.21 conditioner were calibrated to 0.0027 mm/volt (0.01 in./volt) at room temperature and periodically checked with the Schaevitz 41M calibration stand during the testing program. The two RDP LVDTs (s/n 2972 and s/n 2973) have a linear range of 0.25 mm (0.01 in.) and were calibrated initially utilizing gage blocks and the saddle device to secure the LVDTs. The Schaevitz 41M calibration stand was utilized to periodically check the gage calibration during the testing period. The two LVDTs were calibrated to 1.75E-2 and 1.69E-2 mm/volt (6.88E-4 and 6.65E-4 in./volt) at room temperature. The sensitivity of LVDTs is affected by temperature, so calibration also was performed at the testing temperatures.

Compliance Calibration

The compliance λ is defined as u/F, where u is the load-point displacement and F is the load. In linear fracture mechanics, the compliance is useful in determining the crack length for a given geometry and material. The compliance can be transformed into a dimensionless compliance, $g = \lambda EB$, which essentially is independent of material behavior.

For the three-point-bend test, the dimensionless compliance g can be obtained as a function of the dimensionless crack length $\alpha = a/W$. In this project, a curve of g vs α for an aluminum (2024) specimen was obtained experimentally and compared with the theoretical curve, which can be used to determine the crack length of the asphalt concrete (AC) specimens under the three-point-bend test from the loading record. For the three point bend test, K_I is given as (ASTM E399-98):

$$K_I = \frac{F \cdot S}{B \cdot W^{3/2}} f(\alpha) \tag{8}$$

where

$$f(\alpha) = \frac{3\alpha^{1/2}[1.99 - \alpha(1-\alpha)(2.15 - 3.93\alpha + 2.7\alpha^2]}{2(1+2\alpha)(1-\alpha)^{3/2}} \tag{9}$$

The total compliance of the specimen is

$$\lambda = \lambda_{NC} + \lambda_C \tag{10}$$

where λ_{NC} is the compliance of the beam without the crack, and λ_C is the compliance due to the crack; λ_{NC} can be found in an elasticity textbook (16):

$$\lambda_{NC} = [\frac{S^3}{48EI} + \alpha_S \frac{S}{4GA} + \frac{S+25W}{5EBW}] \quad (11)$$

where I is the moment of inertia, G is the shear modulus, A is the cross-sectional area, α_s is the shear factor (for rectangle beams $\alpha_s = 1.2$). To calculate λ_C, the load-point displacement due to the crack can be expressed as

$$u_c = \frac{\partial}{\partial F} \int_0^{aB} G_I d\Gamma \quad (12)$$

where $\Gamma = \xi B$, and ξ is the crack length at a certain time. Combining equations (7) and (8), (12) becomes

$$u_c = \frac{2(1-\upsilon^2)FS^2}{EBW^2} \int_0^{\alpha} f(x)dx \quad (13)$$

where $x = \xi/W$. Therefore, the compliance due to the crack is

$$\lambda_c = \frac{2(1-\upsilon^2)S^2}{EBW^2} H(\alpha) \quad (14)$$

where

$$H(\alpha) = \int_0^{\alpha} f(x)dx = 0.495(1-\alpha)^2 + \frac{0.5853}{\alpha - 1} - 19.38\alpha + 8.717\alpha^2 - 6.098\alpha^3 + \\ + 2.984\alpha^4 - 0.821\alpha^5 + \frac{5.194}{1+2\alpha} - 2.285\ln(1-\alpha) + 13.539\ln(1+2\alpha) - 5.1037 \quad (15)$$

From equation (11) and (14), considering $G = E/[2(1 + \nu)]$, $I = BW^3/12$, and $A = BW$, the total compliance can be represented as

$$\lambda = \frac{S^3}{4BEW^3} + \alpha_s \frac{S(1+\upsilon)}{2BEW} + \frac{S+25W}{5EBW} + \frac{2(1-\upsilon^2)S^2}{BEW^2} H(\alpha) \quad (16)$$

The dimensionless compliance is $g = \lambda EB$, so

$$g = \frac{S^3}{4W^3} + \alpha_s \frac{S(1+\upsilon)}{2W} + \frac{S+25W}{5W} + \frac{2(1-\upsilon^2)S^2}{W^2} H(\alpha) \quad (17)$$

An aluminum (2024) specimen with varying a (0.25, 0.3, 0.35, 0.4, 0.425, 0.45, 0.475, 0.5, 0.525, 0.55) was loaded using the three-point-bend fixture. The span was 226.1 mm (8.9 in.), the width was 50.8 mm (2 in.), and the thickness was 25.4 mm (1 in.). Young's modulus was determined to be 72.4 GPa (10,500 ksi) and Poisson's ratio was 0.32. The dimensional compliance g can be calculated from the linear part of load-load point displacement record for various crack lengths. Figure 4 shows the results between theory and experiment, which are in good agreement for $a/W < 0.4$.

Once the expression for the dimensionless compliance g was established, an indirect method to determine Young's modulus E is available. The initial geometry, including notch length, is well known so that g can be calculated. The initial compliance λ_i can be measured from repeated load-unload cycles within the elastic response of the material, as shown in Figure 5, where the unload-reload loops are seen at the start of the test. With an accurate measure of λ the Young's modulus E is simply $g/\lambda B$.

Unloading was performed in the post-peak region to obtain multiple estimates of the fracture resistance. By measuring the compliance, the crack length can be determined and the toughness can be calculated. Thus, a single specimen was utilized to obtain a crack resistance curve – fracture toughness versus change in crack length.

Materials

A standard MnDOT mix (type 2341, asphalt grade of 85/100) was used in the study. The beams of asphalt concrete were compacted through static compaction with a 1 MN (220 kips) hydraulic load frame. A casting mold 355.6 x 76.2 x 95.25 mm (14 x 3 x 3.75 in.) fabricated from 13 mm (0.5 in.) steel plates was used for all specimen preparation. The air void level varied between 7% and 14% and was achieved by placing the hot (150°C) mix in three lifts, and compressing the asphalt at 450 kN (100 kips) for 60 - 120 s. The specimens were allowed to cool at room temperature for about four hours, and were then placed in an environmental chamber where a temperature of 0°C was achieved gradually over a period of four hours. Approximately one day prior to testing, the temperature of the chamber was adjusted to the testing temperature.

The SENB geometry used in the described study is extensively used in metals; however, its application to asphalt mixtures is restricted due to the sample preparation requirements. The compaction method of choice for asphalt mixtures in the U.S. and Canada is the gyratory compactor (17). Most of the traditional research on asphalt mixtures employs tests performed on cylindrical specimens. The shape of the cores extracted form already built pavements is also cylindrical. Therefore, preparing beams of asphalt mixtures requires additional expensive equipment, such as a slab compactor and would make further comparison of material properties obtained from different testing configurations impossible. As a consequence, most of the asphalt mixtures fracture investigations are based on cylindrical or semi-cylindrical specimens. The current research effort in progress at the University of Minnesota uses semicircular samples following the method proposed by Molenaar (18).

RESULTS

To avoid the inconsistency of the material response near the transition temperature of 0°C, only the temperatures of -18° and -34°C were considered for fracture testing. A total of

twelve specimens were prepared at an air voids content of approximately 10%. Due to experimental difficulties with the load-point displacement, only seven tests are reported (see Table 1).

Although the data suggest that the fracture toughness of this material is the same at the two temperatures, an examination of the loading records gives a clearer picture (Figures 5a and 5b). The geometry, including notch length, was virtually the same for all the specimens, so peak load is directly related to the fracture toughness (the offset method of ASTM was not used to compute K_{Ic}). Substantial nonlinear displacement prior to peak load is evident for the - 18°C test, where the load-point displacement (LPD) at peak load is 0.07 mm. The displacement (LPD) at peak for the -34°C test is only 0.035 mm. The increased nonlinear displacement at the higher temperature contributes to the energy consumption in creating new surfaces, but this additional energy is not included in the calculation of K_{Ic}. Further work is needed to quantify this behavior. It can be stated, however, that the energy needed to initiate a fracture is less at -34°C than at -18°C.

By using the closed-loop testing system, crack propagation can be followed after peak load, and multiple measurements of fracture toughness can be determined from the compliance technique. The specimen is unloaded and reloaded at different stages of displacement; from the slope of the unloading portion the crack length can be estimated. Table 2 shows the results from the unloading-reloading, and Figure 6 is a plot of the data. An increase in fracture toughness with crack length is apparent, and this behavior is displayed by other brittle materials such as rock (19). The plateau of the curves is probably more representative of the asphalt concrete's resistance to fracture than the initial values because of the inelastic zone at the crack tip. Limited tests performed at -18°C for specimens prepared at two different air voids content— 7% and 13% showed, as expected a higher toughness for the lower air voids mixture: $K_{Ic\text{-}7\%}$ = 0.7 MPa-$m^{0.5}$while $K_{Ic\text{-}13\%}$ = 0.2 MPa-$m^{0.5}$.

SUMARRY AND CONCLUSIONS

Closed-loop, computer-controlled fracture tests were conducted using an unload-reload procedure so that multiple measurements of fracture toughness K_{IC} could be obtained from a single specimen in three-point bending. As with any bend test, an accurate measurement of the load-point displacement is complicated by nonlinear deformation and crushing at the roller to specimen contacts. These factors were eliminated by measuring a differential displacement: the deflection of the notch relative to points directly above the supports provides a displacement that avoids the contact problem. This method provides an estimate of Young's modulus E through a compliance calibration.

The behavior (E and K_{Ic}) of the asphalt concrete tested at an air voids content of about 10% was dependent upon temperature. Assuming linear fracture mechanics is valid, the fracture toughness was found to be 0.5 MPa-$m^{0.5}$ at -18°C and at -34°C. However, the loading records indicate that nonlinear behavior is more pronounced at -18°, which means that more energy would be needed to initiate the fracture. In terms of pavement performance, this asphalt concrete would be more resistant to cracking at -18° than at -34°C. The air void content influences the asphalt's fracture toughness. For tests conducted at -18°C, specimens prepared at a lower air voids (7%) exhibited K_{Ic} of 0.7 MPa-$m^{0.5}$, while at higher air voids K_{Ic} was 0.2 MPa-$m^{0.5}$.

Further research is needed to investigate the potential of using this method for obtaining R-curves of asphalt mixtures, which will offer a better understanding of the fracture behavior as compared to single toughness values. This may provide a basis to analyze pavement structures for conditions leading to failure due to cracking.

REFERENCES

1. Dongre, R., Sharma, M.G., Anderson, D.A., "Development of Fracture Criterion for Asphalt Mixtures at Low Temperatures," Transportation Research Record 1228, pp. 94-105, 1989.
2. Lee, N. K. and S. A. M. Hesp, "Low Temperature Fracture Toughness of Polyethylene-Modified Asphalt binders." Transportation Research Record 1436, pp. 54-59, 1994.
3. Lee, N. K., G. R. Morrison, et al. (1995). "Low Temperature Fracture of Poluethylene-Modified Asphalt binders and Asphalt Concrete Mixes." Journal of the Association of Asphalt Paving Technologists **64**: 534-574.
4. Standard Test Method for Plane Strain Fracture Toughness for Metallic Materials (ASTM Method E399-90), Annual book of ASTM Standards, Part 10. American Society for Testing and Materials, Philadelphia, PA 506-515 (1992).
5. Champion, L., Gerard, J.F., Planche, J.P., Martin, D., Anderson, D.A., "Low-Temperature Rheological and Fracture Properties of Polymer-Modified Bitumens," 2nd Eurasphalt and Eurobitume Congress, Barcelona, 2000.
6. Anderson, D. A., Champion – Lapalu, L., Marasteanu, M. O., Le Hir, Y., Martin, D., Planche, J. P., "Low-temperature Thermal Cracking of Bitumens as Ranked by Strength and Fracture Properties," Transportation Research Record 2001, in press.
7. Roy, S. D. and S. A. M. Hesp (2001). "Fracture Energy and Critical Crack Tip Opening Displacement: Fracture Mechanics Based Failure Criteria for Low-Temperature Grading of Asphalt Binders," Journal of the Canadian Association of Asphalt Paving Technologists, accepted for publication.
8. Wells, A. A. (1962). "Unstable Crack Propagation in Metals," Proceeding of the Crack Propagation Symposium Cranfield, The College of Aeronautics, Cranfield, England.
9. Ewalds, H. L. and R. J. H. Wanhill (1985). Fracture Mechanics. Delft, Holland.
10. Roque, R., z. Zhang, et al. (1999). "Determination of Crack Growth Rate Parameters of Asphalt Mixtures Using the Superpave IDT." Journal of the Association of Asphalt Paving Technologists **68**: 404-433.
11. Zhang, Z., R. Roque, et al. (2001). "Evaluation of laboratory Measured Crack Growth rate for asphalt Mixtures," Transportation Research Board, 80th Annual Meeting, Washington, D.C.
12. Labuz, F. J., Dai, S., "Cracking of Asphalt Concrete at Low Temperatures," Final Report, Minnesota Department of Trnasportation, October 1994.
13. Schmidt, R.A. (1976) Fracture toughness testing of limestone. Exp. Mech. 16, pp. 161-167.
14. Schmidt, R.A. and Lutz, TJ. (1979) K_{Ic} and J_{Ic} of Westerly granite- effects of thickness and in-plane dimensions. Fracture mechanics applied to brittle materials. ASTM STP 678, pp. 166-182.
15. Irwin, G.R., and Kies, J.A. (1954) Critical energy rate analysis of fracture strength, Welding Research Supplement 19, pp. 193-198.
16. Sokolnikoff, I.S. (1956) Theory of elasticity, McGraw-Hill.

17. "TP4-00, Method for Preparing and Determining the Density of Hot-Mix Asphalt (HMA) Specimens by Means of the Superpave Gyratory Compactor," AASHTO Provisional Standards, Washington, D.C.: American Association of State Highway Transportation Officials, April 2000 edition.
18. Molanaar, J. M. M. and A. A. A. Molanaar (2000). Fracture Toughness of Asphalt in the Semi-Circular bend Test. 2000 Eurasphalt and Eurobitume Congress, Bacelona, Spain.
19. Labuz, J.F., Shah, S.P., and Dowding, C.H. (1985) Experimental analysis of crack propagation in granite. Int. J. Rock Mech. Min. Sci., Vol. 22(2), pp. 85-98.

TABLE CAPTIONS

Table 1. Experimental results.
Table 2. Results from un-loading re-loading.

FIGURE CAPTIONS

Figure 1a. Elastic behavior in a fracture test.
Figure 1b. Inelastic behavior in a fracture test.
Figure 2. Reference frame for load-point displacement (shown for core specimen).
Figure 3. LVDT platen and yoke (shown for core specimen).
Figure 4. Compliance calibration of the three point bending beam.
Figure 5a. Load record from fracture test at -18°C.
Figure 5b. Load record from fracture test at -34°C.
Figure 6. Change in fracture toughness with crack length.

Table 1. Experimental results.

Specimen	Temp °C	Peak load kN	K_{Ic} MPa-$m^{0.5}$	E_{beam} GPa
3	-18	1.30	0.62	9.74
5	-18	1.09	0.47	10.42
8	-18	1.12	0.51	11.44
9	-34	1.15	0.49	-
10	-34	1.27	0.54	14.67
11	-34	1.23	0.52	-
12	-34	1.13	0.48	-

Table 2. Results from unloading-reloading.

Specimen	Unload-reload cycle	Crack length, a mm	K_{Ic} MPa-$m^{0.5}$
3	8	21.8	0.52
	9	25.7	0.62
	10	30.8	0.67
5	8	23.4	0.47
	9	23.8	0.45
	10	25.4	0.48
8	8	24.4	0.51
	9	26.9	0.56
	10	28.6	0.61
10	8	23.4	0.54
	9	28.3	0.60
	10	34.6	0.68

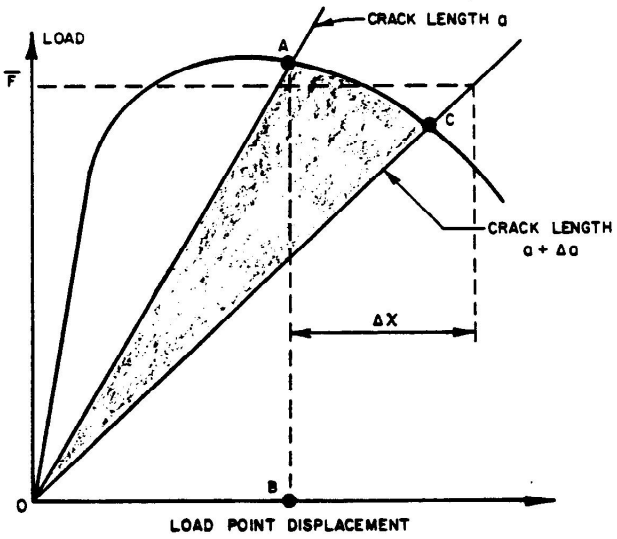

Figure 1a. Elastic behavior in fracture test.

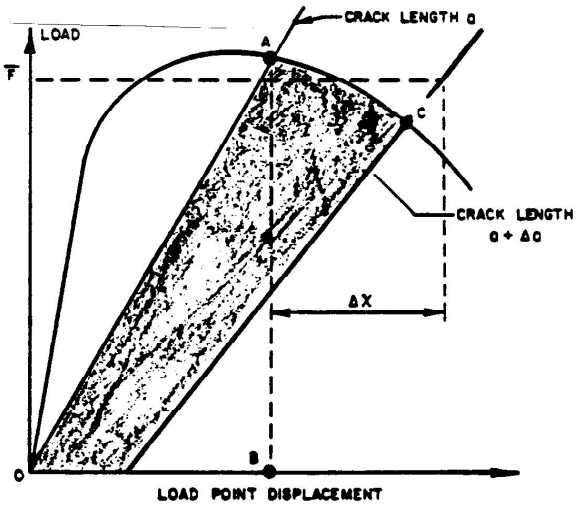

Figure 1b. Inelastic behavior in fracture test.

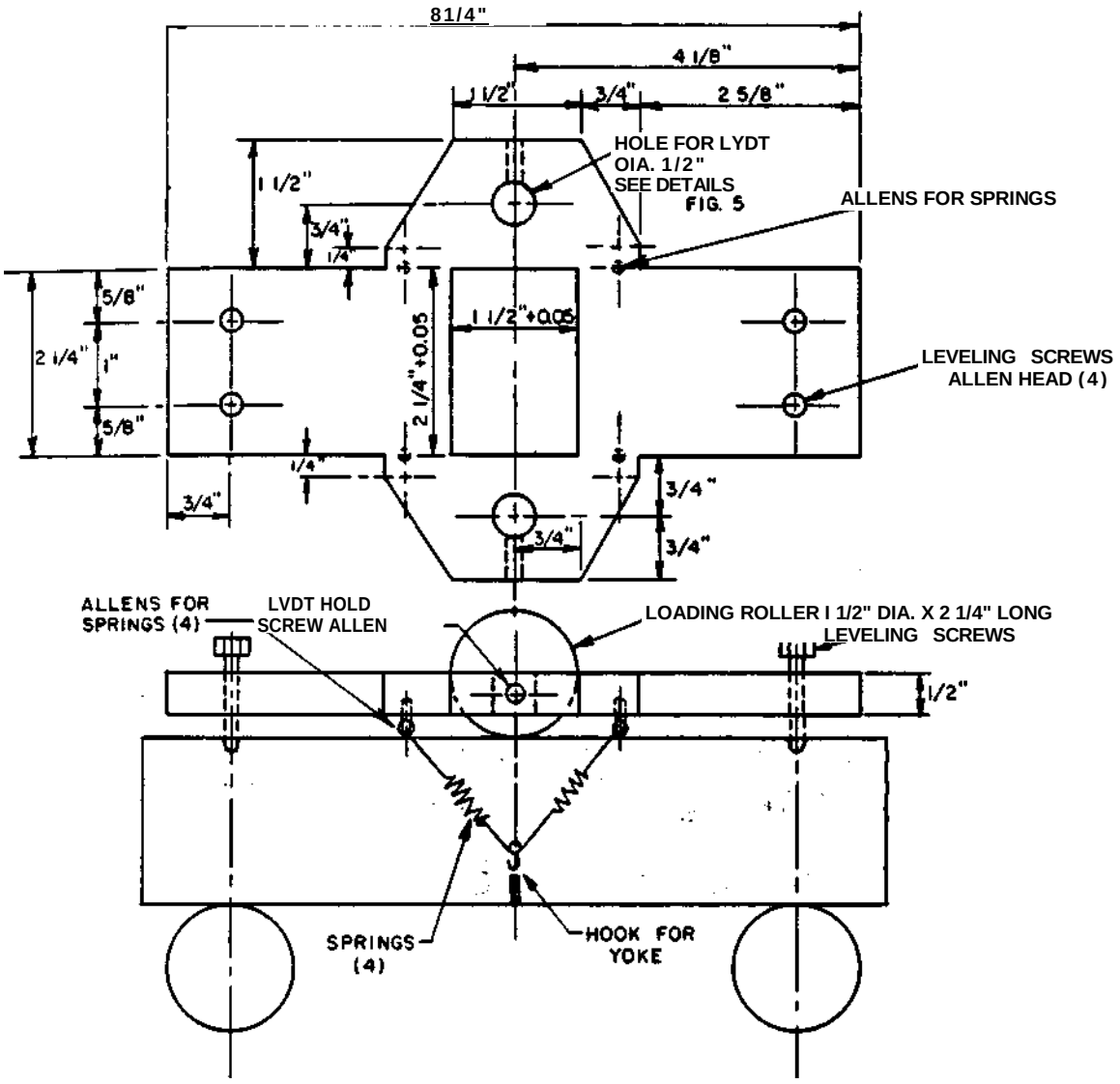

Figure 2. Reference frame for load-point displacement (shown for core specimens).

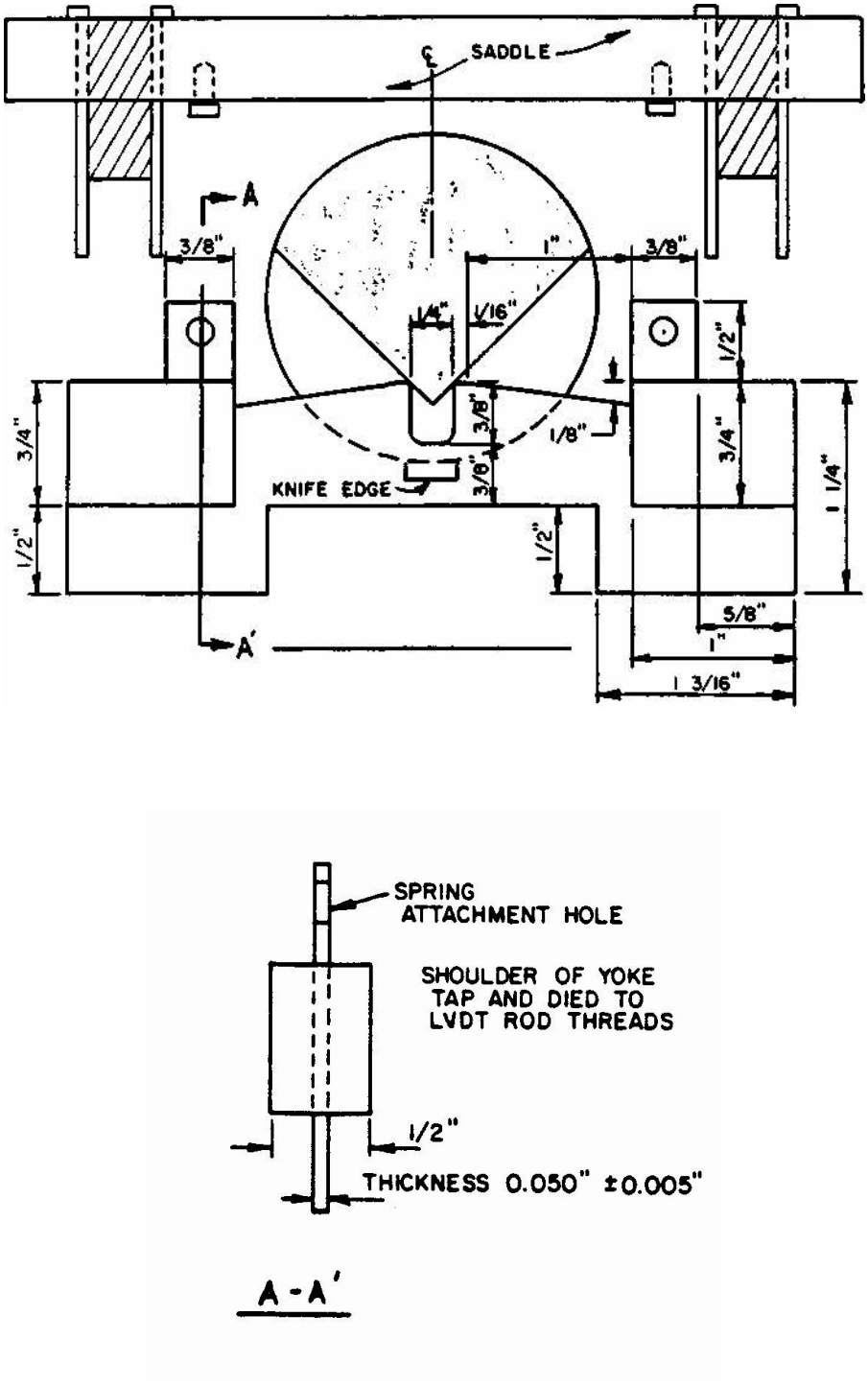

Figure 3. LVDT platen and yoke (shown for core specimens).

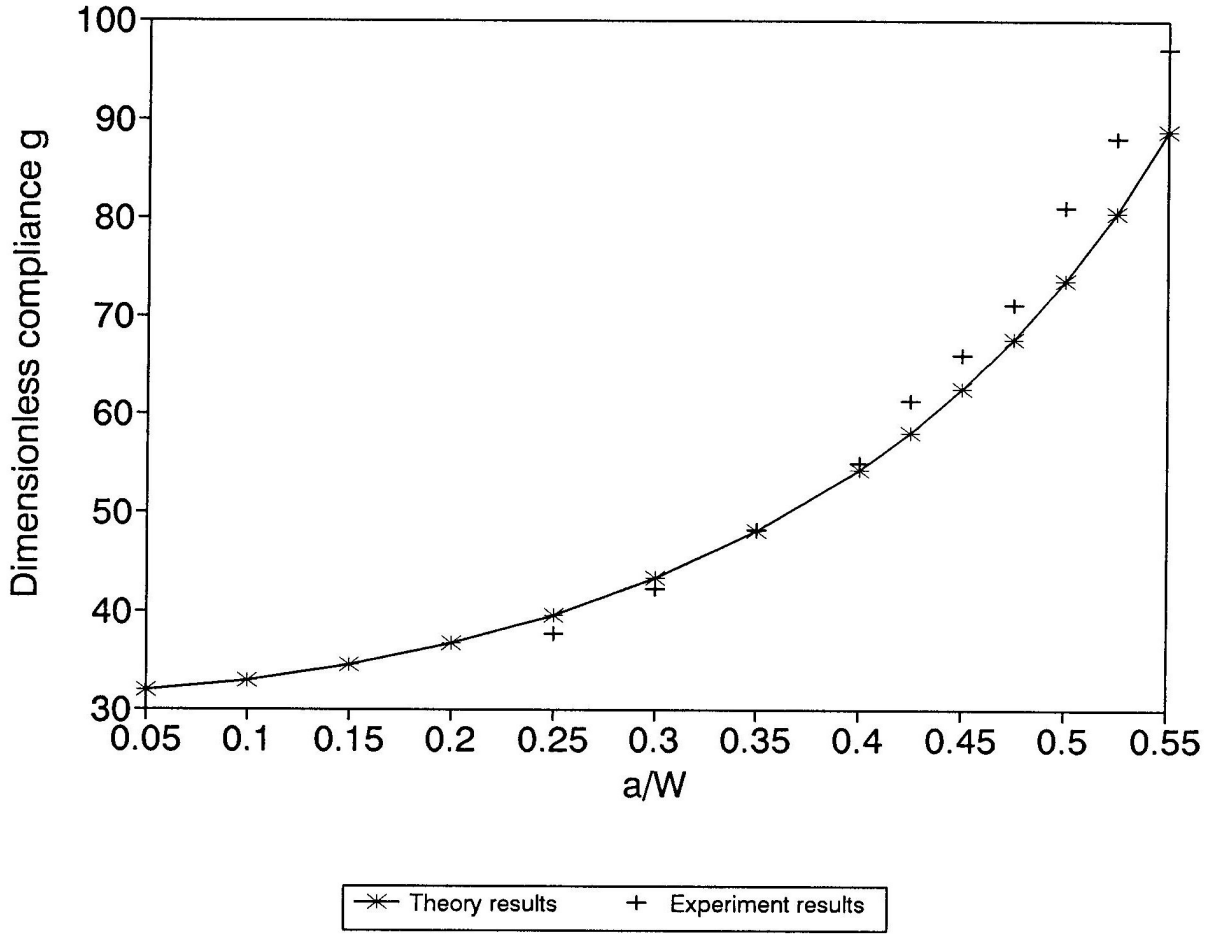

Figure 4. Compliance calibration for the three-point-bend beam.

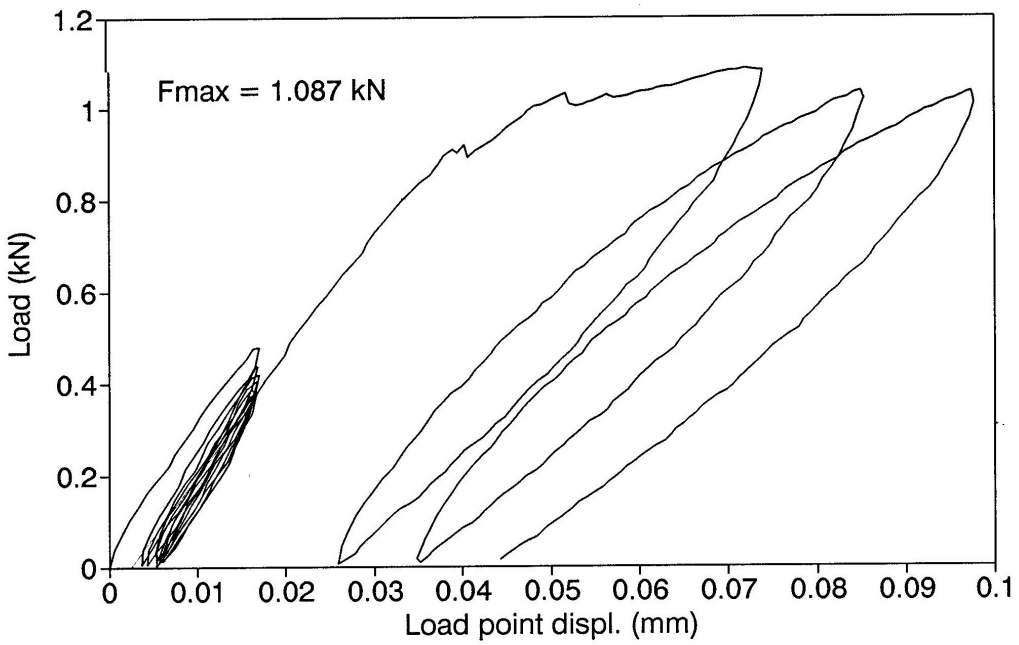

Figure 5a. Load record from fracture at –18°C.

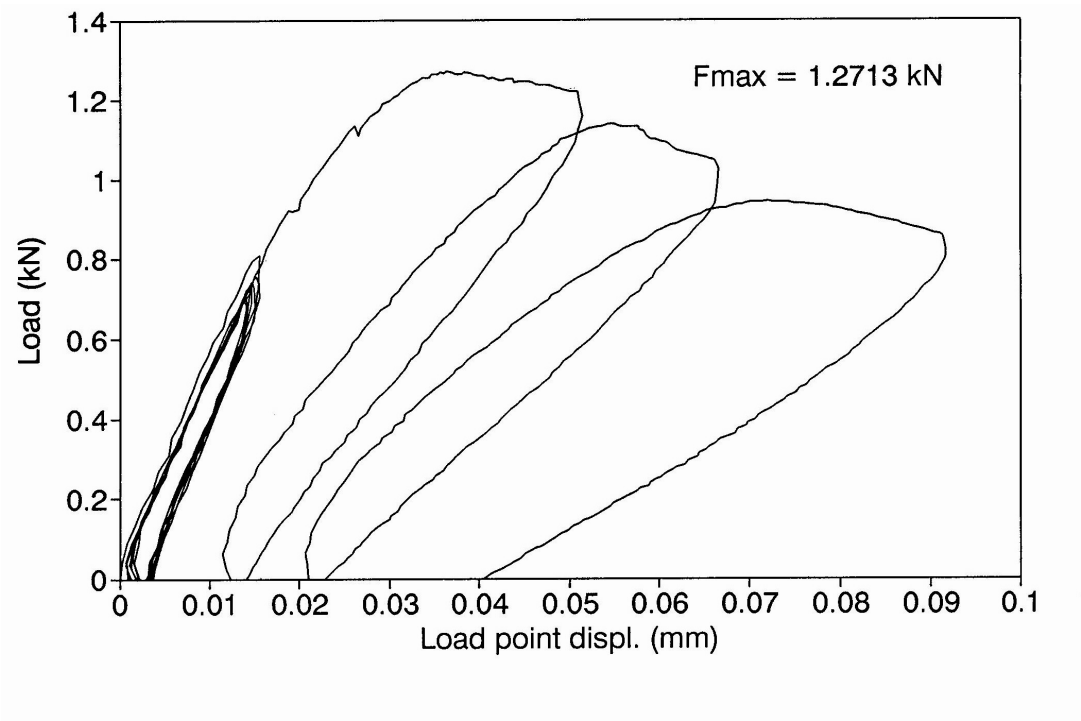

Figure 5b. Load record from fracture at –34°C.

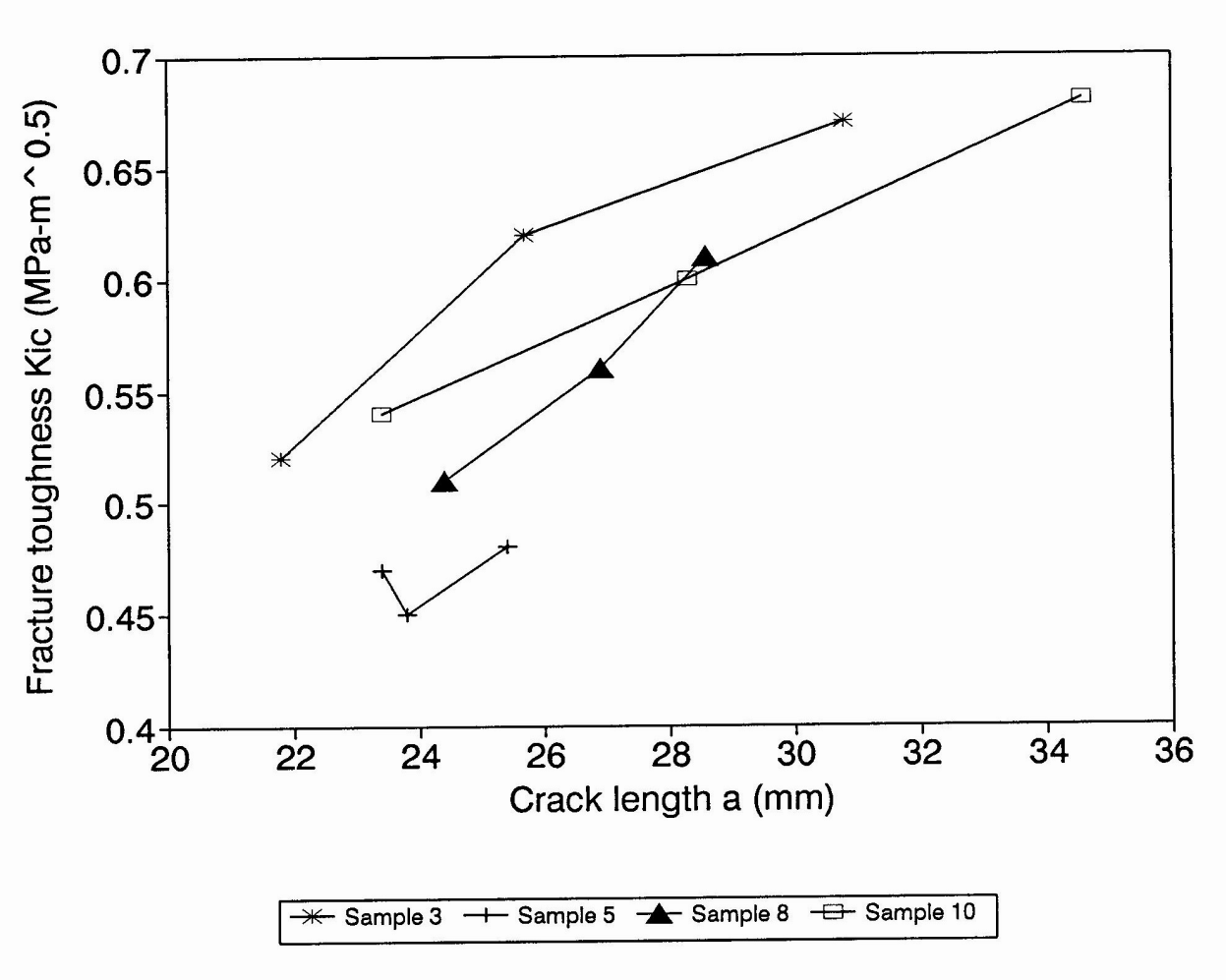

Figure 6. Change in fracture toughness with crack length.